journal of the mechanical behavior of biomedical materials 141 (2023) 105776

Contents lists available at ScienceDirect

Journal of the Mechanical Behavior of Biomedical Materials

journal homepage: www.elsevier.com/locate/jmbbm

The risk of fragment penetrating injury to the heart

Hirotaka Tsukada [a], Thuy-Tien N. Nguyen [a], John Breeze [a,b], Spyros D. Masouros [a,*]

[a] Department of Bioengineering, Imperial College London, UK
[b] Royal Centre for Defence Medicine, Queen Elizabeth Hospital Birmingham, UK

ARTICLE INFO

Keywords:
Secondary blast injury
Penetrating injury
Depth of penetration
Survival analysis
Injury-risk curve
Lamb heart

ABSTRACT

Injury due to the penetration of fragments into parts of the body has been the major cause of morbidity and mortality after an explosion. Penetrating injuries into the heart present very high mortality, yet the risk associated with such injuries has not been quantified. Quantifying this risk is key in the design of personal protection and the design of infrastructure.

This study is the first quantitative assessment of cardiac penetrating injuries from energised fragments. Typical fragments (5-mm sphere, 0.78-g right-circular cylinder and 1.1-g chisel-nosed cylinder) were accelerated to a range of target striking velocities using a bespoke gas-gun system and impacted ventricular and atrial walls of lamb hearts. The severity of injury was shown to not depend on location (ventricular or atrial wall). The striking velocity with 50% probability of critical injury (Abbreviated Injury Scale (AIS) 5 score) ranged between 31 and 36 m/s across all 3 fragments used. These findings can help directly in reducing morbidity and mortality from explosive events as they can be implemented readily into models that aim to predict casualties in an explosive event, inform protocols for first responders, and improve design of infrastructure and personal protective equipment.

1. Introduction

Injury caused by energised fragments following an explosion – termed secondary blast injury – has been the most common cause of trauma in incidents where explosives have detonated (Edwards et al., 2016; Magnus et al., 2018; Yasin et al., 2012). In terrorist bombings between 1970 and 2014, it has been documented that half of the blast injuries were caused by the secondary blast mechanism (Edwards et al., 2016). Preformed metal fragments housed within explosive devices (Singh et al., 2016a) or those produced from the device casing have been estimated to be propelled with initial velocities of approximately 1800 m/s, whilst velocities of up to 600 m/s when reaching a casualty have been suggested to be survivable (Bowen and Bellamy, 1988).

Torso penetrating injuries due to energised fragments are common in civilian mass-casualty events (Peleg et al., 2004) or indeed for non military personnel in conflict zones due to no protective armour worn. All patients except one who had torso injuries sustained penetrating injuries in the Ankara bombing (Yazgan and Aksu, 2016) and 11 out of 17 patients had abdominal penetrating injuries in Hadera bombings (Turégano-Fuentes et al., 2014). Torso penetration that reaches vital organs is associated with high mortality, but few experimental studies exist that correlate what has been seen clinically (Yasin et al., 2012; Turégano-Fuentes et al., 2014; Campbell et al., 1997).

Penetrating cardiac injury is a highly lethal event; the mortality rate - including stab wounds, gunshot wounds and secondary blast injuries - has been estimated at 94% before arrival at hospital and 50% in admitted patients (Campbell et al., 1997). Energy loss of spherical projectiles through the porcine heart at striking velocities between 200 and 900 m/s has been reported before (Humphrey et al., 2018a, 2018b), but it is unclear how these relate to the probability of human penetrating cardiac injury.

Injury models for the penetration of energised fragments are used to inform the design of public infrastructure, the setting up of protocols for emergency response to mass casualty events, and in the design of personal protective equipment. Historically, the assumption in such models is that penetration anywhere near the heart is unsurvivable, which is an over-simplification. Newer models with higher fidelity incorporate individual anatomical structures, such as the heart, using geometries derived from CT scans. Quantitative assessment of cardiac injuries can be conducted using a clinical scoring system such as the Abbreviated injury scale (AIS), which is a clinical tool to classify injury severity. In the AIS, cardiac laceration without perforation and perforation through

* Corresponding author. Department of Bioengineering, Imperial College London, White City Campus, London, SW7 2AZ, UK.
E-mail address: s.masouros04@imperial.ac.uk (S.D. Masouros).

https://doi.org/10.1016/j.jmbbm.2023.105776
Received 6 September 2022; Received in revised form 24 February 2023; Accepted 10 March 2023
Available online 11 March 2023

the cardiac wall attain a score of 3 (serious) and 5 (critical), respectively (Gennarelli and Wodzin, 2008).

This study aims to quantify the risk of a cardiac penetrating injury from a variety of relevant energised projectiles. Cardiac injury-risk curves were developed by accelerating fragments to a range of striking velocities upon fresh and freshly frozen lamb hearts.

2. Materials and methods

Fresh and fresh-frozen lamb hearts were chosen for this study as the material properties of the tissue and the thickness of the ventricular wall are similar to those of the human heart (Sommer et al., 2015; Foale et al., 1987; Karimi et al., 2008; Javani et al., 2016). Fresh lamb hearts were obtained from a local abattoir at the time of slaughter. During transport, each sample was placed in a plastic bag filled with Dulbecco's Modified Eagle Medium (DMEM) and stored in an insulated bag with ice. Upon arrival at the laboratory, each sample was stored in the refrigerator and kept at 4 °C in DMEM until testing. All fresh lamb hearts were tested within 48 h of slaughter to minimise degradation of the tissue. Fresh-frozen lamb hearts were also used in this study; these were thawed fully at room temperature prior to testing.

A 32-mm bore gas-gun system was used to propel a fragment simulating projectile (FSP) towards the target (Nguyen et al., 2019) (Fig. 1). Steel spheres, right-circular (RC) cylinders and chisel-nosed (CN) cylinders were used (Singh et al., 2016b; Breeze et al., 2013a; NATO Standardization Office, 2015) (Table 1). The FSP was carried by the sabot and accelerated using compressed gas through the barrel of the gas-gun system. The FSP was detached from the sabot at the sabot stripper and impacted the sample. The striking velocity of the FSP was calculated from the footage of a high-speed camera (Phantom VEO 710, Vision Research, United States).

The sample, whilst in a thin plastic bag, was clamped onto the mounting apparatus as shown in Fig. 1. The polycarbonate mounting apparatus had holes cut out at entrance and exit to allow the flight of the FSP through the tissue. To investigate the effect of the presence of a plastic bag, tests were performed on plastic bags filled at the bottom with 200 g of water, which was of similar mass to that of a lamb heart. The velocities of the 5-mm sphere before and after passing through the bag showed that the kinetic energy absorbed by the plastic bag was negligible for the tested range of striking velocities between 33 and 124 m/s (Supplementary Table 1).

The FSPs were shot into the left and right side of the two cardiac walls, at ventricular and atrial locations (Fig. 2a). The tests were classified as no penetration, penetration into (commensurate with an AIS 3 injury), and perforation through the cardiac wall (commensurate with an AIS 5+ injury) (Fig. 2 b-d). To optimise the use of samples, when considerably shallow penetration or no penetration was observed, an additional FSP was shot into the intact tissue in the same region of the cardiac wall. DoP was measured using radiography (Fluoroscan InSight FD, Hologic Inc., United States). When the projectile perforated the cardiac wall and remained inside the sample (Fig. 2 d), a small steel marker was placed at the entrance of the penetrating wound, and the specimen was scanned on the top, side and front surface; DoP was calculated from the distances between the steel marker and the furthest end of the retained projectile obtained from the three orthogonal scans.

Table 1
The mass and dimensions of the sphere, right-circular (RC) cylinder and chisel-nose (CN) cylinder.

Shape	Material	Mass [g]	Diameter [mm]	Length [mm]
Sphere	Carbon steel	0.51	5	–
RC cylinder	Carbon steel	0.78	4.5	6.3
CN cylinder	Carbon steel	1.1	5.4	6.4

In order to ascertain the effect of a freeze-thaw cycle and of impact locations on penetration behaviour, 5-mm spheres were shot into different locations of both fresh and frozen-thawed lamb hearts. The linear regressions of the DoP over striking velocities were compared using the statistical software SPSS (version 28, IBM, United States). An analysis of covariance (ANCOVA) was performed using the general linear model univariate procedure to obtain the p-values of their slopes and y-intercepts.

Survival analysis was carried out using the statistical software NCSS (v11, NCSS, United States) to establish injury-risk curves representing the injury probability as a function of the striking velocity. Prior to the survival analysis, a best fit analysis was performed with all experimental data to determine the statistical model of the injury-risk curves based on maximum likelihood values. The normal distribution was identified as the most suitable model for the survival analysis. The corridor of the injury-risk curve was estimated using the 95% confidence interval (CI); when the 95% CI could not be calculated from the survival analysis due to no overlapping data points between striking velocities resulting in tissue perforation and not, the corridor was estimated with the standard deviation using the method suggested in the AEP-2920 NATO standard (NATO Standardization Office, 2015). To compare statistically tissue resistance to perforation between the different locations on the cardiac wall and between storage conditions, the striking velocities at 50% probability of perforation through the cardiac wall (V_{50}) were used and the independent Student's t-test was performed from the arithmetic mean according to the AEP-2920 NATO standard (NATO Standardization Office, 2015). To ascertain whether injury-risk curves of all impact scenarios can be combined in each projectile group, the z-test was performed on striking velocities in the range between 1% and 99% probability of an AIS 5+ injury. The parameters of the z-test such as population mean and 95% CI were obtained from the outcome of the survival analysis.

3. Results

Fifty-five lamb hearts were used to conduct 159, 56 and 53 impact tests using the 5-mm sphere, the 0.78-g-RC cylinder and the 1.1-g-CN cylinders, respectively (Table 2). The left and right of each cardiac wall were targeted in this test; the average thickness of each cardiac wall

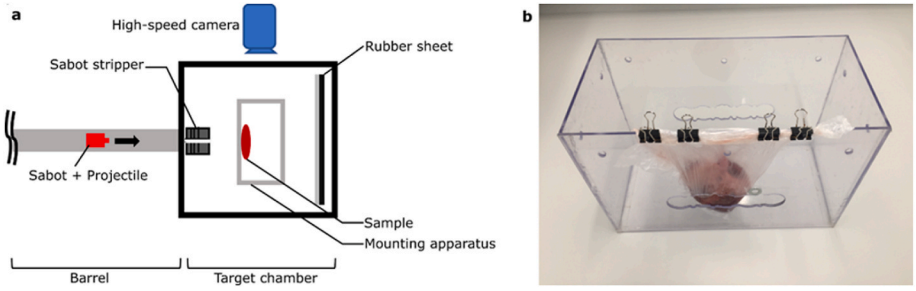

Fig. 1. (a) A schematic of the 32-mm bore gas-gun system and (b) a photograph of the mounting apparatus at the target chamber; the heart is placed in a plastic bag which is suspended with clips from a polycarbonate container.

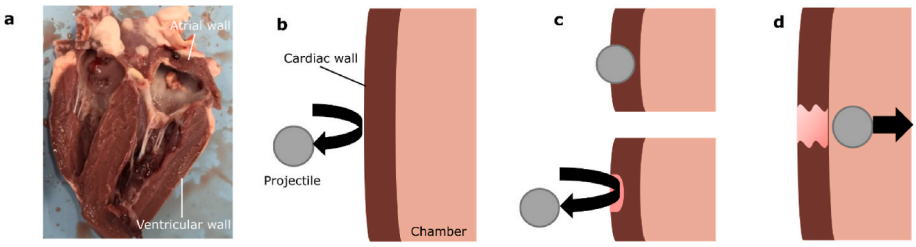

Fig. 2. (a) Section through the lamb heart denoting the locations of atrial and ventricular walls. Test outcomes were classified as: (b) no penetration, when the projectile bounces off the cardiac wall without causing damage; (c) penetration, when the projectile penetrates the cardiac wall but does not come out the other end or when it bounces off the wall causing a shallow wound; and (d) perforation, when the projectile penetrates into and escapes from the cardiac wall into the chamber.

Table 2
Number of impact tests conducted per storage condition, fragment used, and target location.

Sample storage	Projectile	Number of tests			
		Left ventricle	Right ventricle	Left atrium	Right atrium
Fresh	Sphere	33	42	16	12
Freeze and thaw	Sphere	15	14	14	13
	RC cylinder	13	14	13	16
	CN cylinder	13	17	15	8

RC: right-circular, CN: chisel-nosed.

is shown in Table 3.

3.1. Effect of storage and impact conditions

Fig. 3 presents the V_{50} values of cardiac wall perforation using the 5-mm sphere shot into the left and right cardiac walls of the fresh samples. DoP as a function of the striking velocity was measured for the shots whereby the projectile perforated the cardiac wall and came to rest inside the heart (Supplementary Fig. 1). There were no significant differences ($p \geq 0.05$) between the two slopes, intercepts, and V_{50} values for left and right cardiac walls.

Table 4 shows the comparison of the slopes of DoP over FSP-striking velocity and their y-intercepts using the 5-mm spheres for different locations (ventricle and atrium) and storage conditions (fresh and frozen-thawed). There were no significant differences between any pairs of data sets.

Fig. 4 shows the injury-risk curves for an AIS 5+ injury for the 5-mm sphere between the fresh ventricle and fresh atrium; and the fresh and frozen-thawed sample for both impact locations. These striking velocities between 1% and 99% probability of an AIS 5+ injury were compared statistically. There were no significant differences ($p \geq 0.05$) between these velocity values suggesting that there was no difference between the risk curves of the ventricular and atrial wall, and of the fresh and frozen-thawed sample.

Table 3
The thickness of ventricular and atrial walls (mean ± one standard deviation).

Sample	Thickness			
	Ventricular wall [mm]		Atrial wall [mm]	
	Left	Right	Left	Right
Lamb heart	14.05 ± 2.94	8.50 ± 1.70	4.43 ± 1.98	2.91 ± 1.38
Human heart	12.46 ± 3.84[a]	4 ± 1[a]	–	–

[a] The thickness of the human ventricular wall was obtained from existing studies (Sommer et al., 2015; Foale et al., 1987).

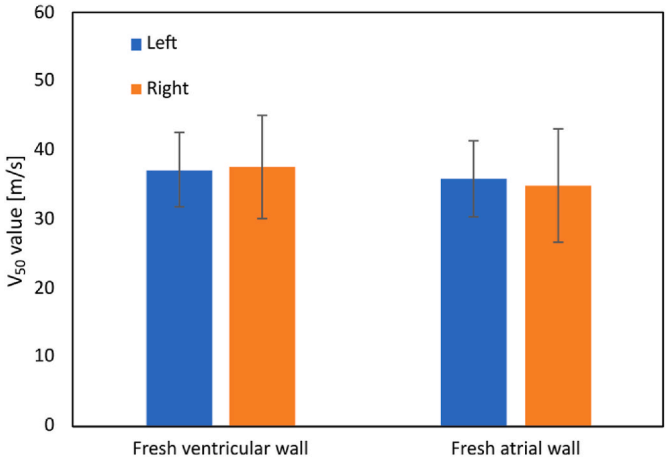

Fig. 3. V_{50} values for cardiac wall perforation by the 5-mm spheres impacting different locations of the fresh heart, with one standard deviation (error bars) as obtained from the method suggested in the AEP-2920 NATO standard [20].

Table 4
Tests of statistical significance under the two storage conditions using the 5-mm sphere projectiles; values show p-values for slope and y-intercept of linear regression, respectively, of the depth of penetration versus striking velocity graphs.

Storage and impact location		Fresh		Freeze and thaw	
		Ventricle	Atrium	Ventricle	Atrium
Fresh	Ventricle		0.14/ 0.28	0.77/ 0.58	0.80/ 0.44
	Atrium	0.14/ 0.28		0.66/ 0.84	0.52/ 0.27
Freeze and thaw	Ventricle	0.77/ 0.58	0.66/ 0.84		0.98/ 0.44
	Atrium	0.80/ 0.44	0.52/ 0.27	0.98/ 0.44	

No significance $p \geq 0.05$.

3.2. Overall ballistic response of cardiac tissue

Fig. 5 shows the combined DoP of the overall ventricle and atrium impacts as a function of the striking velocity for each FSP. The slopes and y-intercepts obtained from tests on ventricular and on atrial walls had no statistical differences ($p \geq 0.05$) for each FSP. Therefore, the linear regression of each graph was estimated from the combined data set of both impact locations.

Fig. 6 shows the injury-risk curves for an AIS 5+ injury to the heart. The V_{50} values (mean ± standard deviation) were 36.1 ± 4.2 m/s for the 5-mm sphere, 33.9 ± 4.8 m/s for the 0.78-g-RC cylinder, and 31.1 ± 3.9 m/s for the 1.1-g-CN cylinder. Supplementary Fig. 2 shows the injury-risk curves of each cardiac wall.

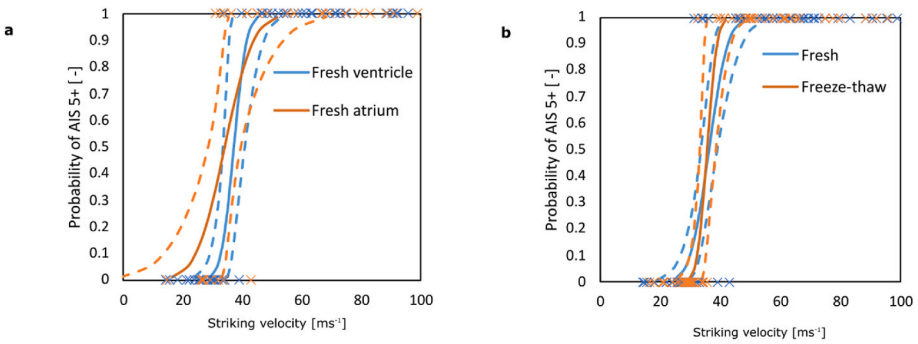

Fig. 4. (a) The injury-risk curves of AIS 5+ for the 5-mm sphere into the fresh ventricle and fresh atrium, and (b) into the overall fresh and overall frozen-thawed sample whereby 'overall' indicates the combined data for both impact locations; the 95% confidence interval corridor of each injury-risk curve is shown with dotted lines.

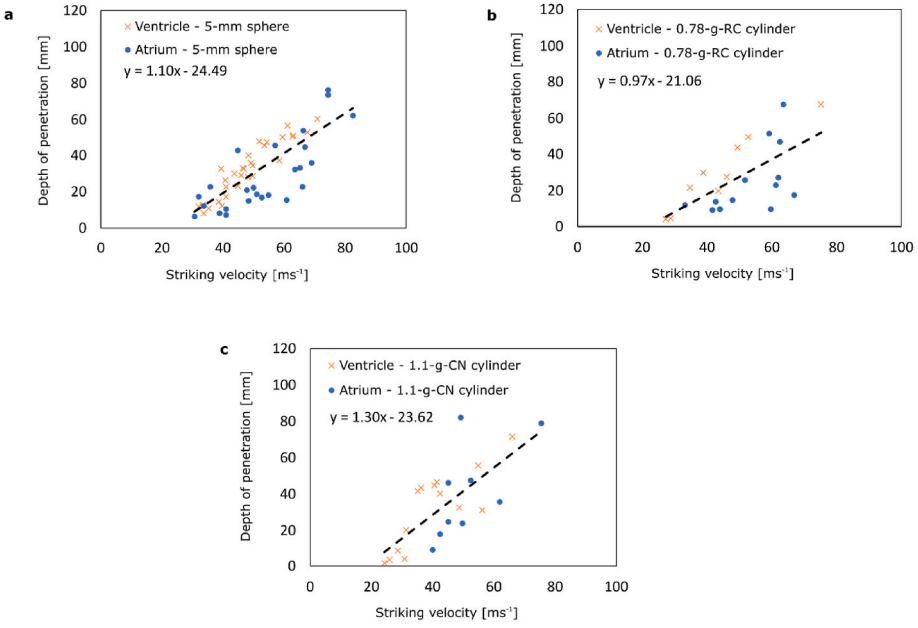

Fig. 5. (a) The depth of penetration into both the fresh and frozen-thawed heart samples using the 5-mm spheres, (b) the frozen-thawed heart samples using the 0.78-g RC cylinders, and (c) the frozen-thawed heart samples using the 1.1-g CN cylinders. Linear regressions were produced from data of both impact locations.

4. Discussion

This study is the first to quantify the risk of penetrating injury into cardiac tissue using 3 types of FSP. Our results show that relatively low striking velocities can cause perforation through the cardiac wall commensurate with an injury which is likely to be critical; the V_{50} value of perforation through the cardiac wall into the chamber is approximately half that into the intercostal muscles against the 0.78 g RC cylinder (33.9 vs. 66 m/s) (Nguyen et al., 2022).

The retardation of the projectile was found to be similar when the projectile impacted ventricular or atrial walls (Supplementary Fig. 1 and Table 4). Even though the trajectory of the projectile post perforation was dependent on impact location, no significant differences were found in the slopes of DoP against striking velocity and their y-intercepts between all impact locations. These findings support that the data sets of both ventricle and atrium impacts, for both left and right sides, can be combined into a single linear regression (Fig. 5). Some projectiles stroke the atrium at the dense connective tissue of the cardiac valve adjacent to the atrial wall. This likely lead to the larger variances of the slopes of the DoP against striking velocity in the atrium impacts, compared to those in the ventricle impacts. The large variance in the DoP of a cylindrical projectile is likely due to the change of the projectile's yaw angle post impact and subsequent tumbling during tissue penetration (Bellamy, 1990) (supplementary video).

Supplementary video related to this article can be found at https://doi.org/10.1016/j.jmbbm.2023.105776

Cardiac laceration with no perforation – classified as an AIS 3 injury (Gennarelli and Wodzin, 2008) – was seen infrequently in this study suggesting that it is an unlikely injury pattern to occur in this mechanism. In the range of 1–99% probability of injury, the striking velocities for penetration into (AIS 3+) and perforation through the cardiac wall (AIS 5+) for the 5-mm sphere were not statistically different (z-test, $p \geq 0.05$) (Supplementary Fig. 3). This suggests that the projectile is highly likely to perforate the cardiac wall if it manages to cut through the surface. Similarly, despite the different thicknesses of ventricular and atrial walls (Table 3), there were no significant differences between the striking velocities at various risks of perforation through ventricular and atrial walls (Fig. 4). This suggests that resistance to perforation through the cardiac wall is similar irrespective of impact location. Therefore, it was possible to combine these data sets to establish a single injury-risk curve for each projectile regardless of the impact location.

Some studies report that the material properties of soft tissue are influenced by a freeze-thaw cycle partly due to the expansion of the water inside the tissue damaging its structure during freezing (Santago

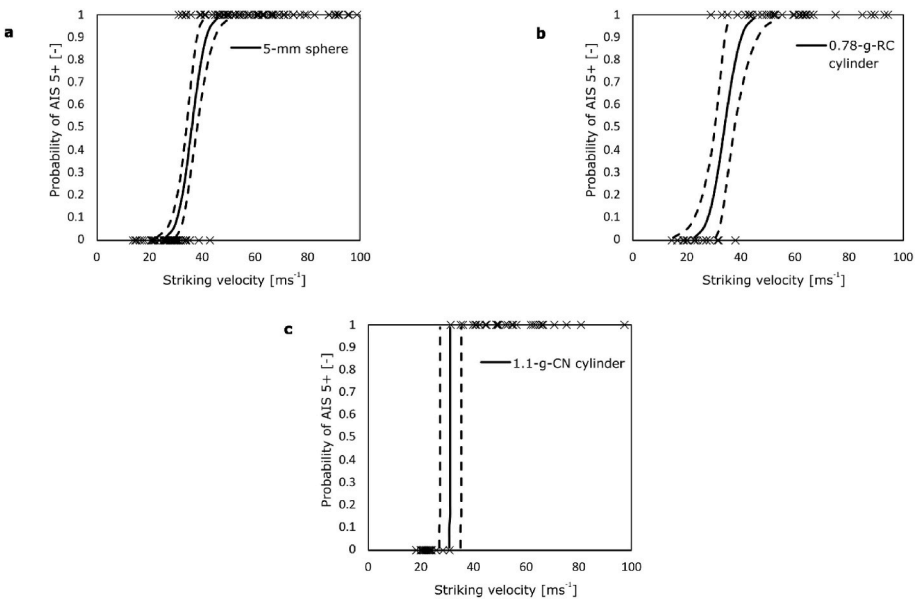

Fig. 6. (a) The injury-risk curves of an AIS 5+ injury for the 5-mm sphere into both the fresh and frozen-thawed heart, (b) for the 0.78-g-RC cylinder into the frozen-thawed heart, and (c) for the 1.1-g-CN cylinder into the frozen-thawed heart. The corridor of each injury-risk curve is denoted with dotted lines representing the 95% confidence interval in (a) and (b) and the standard deviation in (c).

et al., 2009; Dương et al., 2015). Others have found that the material properties of leg ligament and the energy absorption of projectile penetration into the muscle tissue are unaffected by a freeze-thaw cycle (Woo et al., 1986; Breeze et al., 2015). Our results show that the slopes and y-intercepts of DoP against striking velocity and the risk of perforation had no statistical differences across storage conditions. Therefore, one freeze-thaw cycle in this study did not affect the penetration and perforation behaviour of cardiac tissue, which agrees with the findings of the previous study on penetration through muscle tissue (Breeze et al., 2015).

The lamb heart in this study was inserted inside a plastic bag and clamped onto the mounting apparatus without a backing material behind the sample (Fig. 1b). We deemed this mounting to be acceptable in its ability to simulate the *in situ* condition during fragment penetration, as the posterior surface of the heart lies against the aortic arch and spine and so would be loosely supported by these organs in a case of a posterior displacement. The high-speed camera footage of the experiment indeed showed consistently negligible displacement of the heart for the duration of the projectile's motion (that is, till it came to rest in the cardiac wall, within the heart after perforation, or till it bounced off the cardiac wall), thus confirming that the exclusion of a backing material in our setup did not affect the penetration behaviour.

Mass and geometry of FSPs are parameters shown to affect levels of tissue damage (Breeze et al., 2013b) and thus were expected to influence the V_{50} values and the injury-risk curves. Therefore, extensive testing incorporating FSPs spanning relevant mass and geometry envelopes would be required to develop relevant injury-risk curves. The choice of FSPs in this study was based on field data and standard practice in the assessment of armour. In the Boston Marathon bombing, 17 fragments were found in the body of casualties and 5 ball bearings were estimated at approximately 5-mm of diameter using CT scans (Singh et al., 2016b). During UK military operations in Afghanistan, 16 fragments were excised from the neck of soldiers and 8 fragments were identified as cylinders with a mean mass of 0.78 g (Breeze et al., 2013a). Accordingly, the 5-mm steel sphere and 0.78-g-RC steel were considered representative of fragments to study penetrating injuries. Although less relevant to data from recent explosive events, the 1.1-g CN steel cylinder is widely used in ballistic tests and recommended in the AEP-2920 NATO standard (NATO Standardization Office, 2015). Hence, it was also included in this study to allow for comparisons within the defence community with existing, albeit commercially sensitive, data from test houses.

IED fragments would be expected to reach a casualty and the curved boundaries of the heart across a range of yaw angles. A low yaw angle at impact would be retarded during penetration less than a high yaw angle, thus leading to greater DoPs and lower V_{50} values. This study focused on the worst-case scenario, which is associated with low yaw angles. Impacts by the cylindrical projectile at high yaw angles (>60°) were therefore removed from the experimental data here, also due to the high probability of them tumbling during penetration.

Use of a cadaveric animal model to infer behaviour of living human tissue is a limitation of the study. The lamb heart was chosen because the thickness of its ventricular wall and material properties are closer to those of the human heart compared to other animals (Sommer et al., 2015; Foale et al., 1987; Karimi et al., 2008; Javani et al., 2016; Wang et al., 2010; Ghaemi et al., 2009; Omann et al., 2019). The use of fresh and fresh-frozen cadaveric tissue intended to limit any tissue degradation. The muscle tissue in the heart stiffens immediately after death (Shedge et al., 2021) so even the fresh cardiac muscle does not replicate accurately behaviour of living muscle tissue. Therefore, it is likely that the V_{50} values calculated here are slightly underestimated based on this change in material properties. Furthermore, in our cadaveric animal model there was air instead of blood inside the cardiac chambers; the difference in density of the two fluids could have affected the penetration behaviour; from the equation of motion for the 5-mm sphere with an initial velocity of 50 m/s, the estimated DoP of the blood-filled chamber was 5 mm less than that of the air-filled chamber; hence, the DoP of our results was likely slightly overestimated. Approximately 120 ml of blood exist in each ventricle at the end of the diastole (Hall et al., 2021). The periodical change of the overall mass of the heart in itself we estimate would have a minimal effect on the penetration resistance values because of the negligible displacement of the heart that we saw in the high speed video footage during projectile penetration. During the systolic and diastolic cycles, the periodical change of the cardiac wall stress, observed to be between 4 and 17 kPa in the left ventricle (Alter et al., 2016), would likely affect the V_{50} values; specifically, we estimate that tension in the wall would result in a lower V_{50} value. Indeed, investigating how such an increase in cardiac wall stress affects the V_{50} value should be considered in future research.

5. Conclusions

This study is the first quantitative assessment of cardiac penetrating injuries from energised fragments. A 50% probability of DoP commensurate with a critical injury to the heart was found to occur with fragment striking velocities of only 31–36 m/s. Striking location was shown to not affect the probability of injury. The data from this study can be implemented directly into computational models of injury prediction for mass-casualty events and so inform the design of infrastructure, of protocols for emergency responses, and for personal protective equipment.

CRediT authorship contribution statement

Hirotaka Tsukada: Writing – review & editing, Writing – original draft, Investigation, Data curation. **Thuy-Tien N. Nguyen:** Writing – review & editing, Investigation, Data curation. **John Breeze:** Writing – review & editing, Conceptualization. **Spyros D. Masouros:** Writing – review & editing, Conceptualization.

Declaration of competing interest

The authors declare that they have no known competing financial interests or personal relationships that could have appeared to influence the work reported in this paper.

Data availability

Data will be made available on request.

Acknowledgement

This work was conducted in the Royal British Legion Centre for Blast Injury Studies at Imperial College London. The authors would like to acknowledge the financial support of the Royal British Legion and of Defence Medical Services.

Appendix A. Supplementary data

Supplementary data to this article can be found online at https://doi.org/10.1016/j.jmbbm.2023.105776.

References

Alter, P., et al., 2016. Wall stress determines systolic and diastolic function - characteristics of heart failure. Int. J. Cardiol. 202, 685–693.
Bellamy, RF, 1995. Combat trauma overview. In: Zajtchuk, R, Grande, CM (Eds.), Textbook of Military Medicine, Anesthesia and Perioperative Care of the Combat Casualty. Office of the Surgeon General, United States Army, Falls Church, VA, pp. 1–42.
Bowen, T.E., Bellamy, R.F., 1988. Emergency War Surgery. US Department of Defense. https://doi.org/10.1001/archotol.1959.00730030805023.
Breeze, J., et al., 2013a. Characterisation of explosive fragments injuring the neck. Br. J. Oral Maxillofac. Surg. 51, e263–e266.
Breeze, J., James, G.R., Hepper, A.E., 2013b. Perforation of fragment simulating projectiles into goat skin and muscle. J. Roy. Army Med. Corps 159, 84–89.
Breeze, J., Carr, D.J., Mabbott, A., Beckett, S., Clasper, J.C., 2015. Refrigeration and freezing of porcine tissue does not affect the retardation of fragment simulating projectiles. J Forensic Leg Med 32, 77–83.
Campbell, N.C., et al., 1997. Review of 1198 cases of penetrating cardiac trauma. Br. J. Surg. 84, 1737–1740.
Dương, M.T., Nguyễn, N.H., Trần, T.N., Tolba, R.H., Staat, M., 2015. Influence of refrigerated storage on tensile mechanical properties of porcine liver and spleen. Int Biomech 2, 79–88.
Edwards, D.S., McMenemy, L., Stapley, S.A., Patel, H.D.L., Clasper, J.C., 2016. 40 years of terrorist bombings-A meta-analysis of the casualty and injury profile. Injury 47, 646–652.
Foale, R., et al., 1987. Echocardiographic measurement of the normal adult right ventricle. Heart 57, 396.
Gennarelli, T.A., Wodzin, E., 2008. The Abbreviated Injury Scale 2005, Update 2008. American Assoc. for Automotive Med.
Ghaemi, H., Behdinan, K., Spence, A.D., 2009. In vitro technique in estimation of passive mechanical properties of bovine heart. Part I. Experimental techniques and data. Med. Eng. Phys. 31, 76–82.
Hall, J.E., John, E., Hall, M.E., Michael, E., Hall, J.E., John, E., Guyton, A.C., 2021. Guyton and Hall Textbook of Medical Physiology. Textbook of Medical Physiology. Elsevier.
Humphrey, C., Henneberg, M., Wachsberger, C., Kumaratilake, J., 2018a. Comparison of porcine organs and commonly used ballistic simulants when subjected to impact from steel spheres fired at supersonic velocities. Forensic Sci. Int. 288, 123–130.
Humphrey, C., Henneberg, M., Wachsberger, C., Kumaratilake, J., 2018b. The deceleration of a spherical projectile passing through porcine organs at laboratory temperature (16 °C) and core body temperature (37 °C). J Forensic Leg Med 53, 46–50.
Javani, S., Gordon, M., Azadani, A.N., 2016. Biomechanical properties and microstructure of heart chambers: a paired comparison study in an ovine model. Ann. Biomed. Eng. 44, 3266–3283.
Karimi, H., Moghaddam, G., Rezazadeh, F., 2008. In vitro ultrasonography of the normal sheep heart. Pakistan Veterinary Journal (Pakistan) 28, 92–94.
Magnus, D., Khan, M.A., Proud, W.G., 2018. Epidemiology of civilian blast injuries inflicted by terrorist bombings from 1970-2016. Defence Technology 14, 469–476.
NATO Standardization Office, 2015. AEP 2920 – Procedures for the Evaluation and Classification of Personal Armour, Bullet and Fragmentation Threats. Edition A. Preprint at, Version 1.
Nguyen, T.T., et al., 2019. Experimental platforms to study blast injury. J. Roy. Army Med. Corps 165, 33–37.
Nguyen, T.-T.N., Breeze, J., Masouros, S.D., 2022. Penetration of energized metal fragments to porcine thoracic tissues. J. Biomech. Eng. 144, 1–9.
Omann, C., et al., 2019. Resolving the natural myocardial remodelling brought upon by cardiac contraction; A porcine ex-vivo cardiovascular magnetic resonance study of the left and right ventricle. J. Cardiovasc. Magn. Reson. 21, 1–19.
Peleg, K., et al., 2004. Gunshot and explosion injuries: characteristics, outcomes, and implications for care of terror-related injuries in Israel. Ann. Surg. 239, 311–318.
Santago, A.C., Kemper, A.R., McNally, C., Sparks, J.L., Duma, S.M., 2009. Freezing affects the mechanical properties of bovine liver. Biomed. Sci. Instrum. 45, 24–29.
Shedge, R., Krishan, K., Warrier, V., Kanchan, T., 2021. Postmortem Changes. StatPearls Publishing, Treasure Island (FL).
Singh, A.K., et al., 2016a. Blast injuries: from improvised explosive device blasts to the Boston Marathon bombing. Radiographics 36, 295–307.
Singh, A.K., Sodickson, A., Abujudeh, H., 2016b. Imaging of abdominal and pelvic injuries from the Boston Marathon bombing. Emerg. Radiol. 23, 35–39.
Sommer, G., et al., 2015. Biomechanical properties and microstructure of human ventricular myocardium. Acta Biomater. 24, 172–192.
Turégano-Fuentes, F., Pérez-Diaz, D., Sanz-Sánchez, M., Alfici, R., Ashkenazi, I., 2014. Abdominal blast injuries: different patterns, severity, management, and prognosis according to the main mechanism of injury. Eur. J. Trauma Emerg. Surg. 40, 451–460.
Wang, B., et al., 2010. Fabrication of cardiac patch with decellularized porcine myocardial scaffold and bone marrow mononuclear cells. J. Biomed. Mater. Res. 94, 1100–1110.
Woo, S.L.Y., Orlando, C.A., Camp, J.F., Akeson, W.H., 1986. Effects of postmortem storage by freezing on ligament tensile behavior. J. Biomech. 19, 399–404.
Yasin, M.M.A., Nasreen, G., Malik, S.A., 2012. Injury pattern of suicide bomb attacks in Pakistan. Eur. J. Trauma Emerg. Surg. 38, 119–127.
Yazgan, C., Aksu, N.M., 2016. Imaging features of blast injuries: experience from 2015 Ankara bombing in Turkey. Br. J. Radiol. 89.